Cogent Engineering

ISSN: (Print) (Online) Journal homepage: www.tandfonline.com/journals/oaen20

Tribological simulation analysis of artificially aged A356 alloy with minor addition of copper and zinc

Nithesh K, Gowrishankar M C, Sathyashanakara Sharma, Ananda Hegde, Shamanth Bhat M, Rajesh Nayak & Srinivas D

To cite this article: Nithesh K, Gowrishankar M C, Sathyashanakara Sharma, Ananda Hegde, Shamanth Bhat M, Rajesh Nayak & Srinivas D (2024) Tribological simulation analysis of artificially aged A356 alloy with minor addition of copper and zinc, Cogent Engineering, 11:1, 2344118, DOI: 10.1080/23311916.2024.2344118

To link to this article: https://doi.org/10.1080/23311916.2024.2344118

Published online: 25 Apr 2024.

COGENT ENGINEERING
2024, VOL. 11, NO. 1, 2344118
https://doi.org/10.1080/23311916.2024.2344118

MATERIAL ENGINEERING | RESEARCH ARTICLE

OPEN ACCESS Check for updates

Tribological simulation analysis of artificially aged A356 alloy with minor addition of copper and zinc

Nithesh K[a,b], Gowrishankar M C[a], Sathyashanakara Sharma[a], Ananda Hegde[a], Shamanth Bhat M[a], Rajesh Nayak[a] and Srinivas D[a]

[a]Department of Mechanical and Industrial Engineering, Manipal Institute of Technology, Manipal Academy of Higher Education, Manipal, India; [b]Department of Mechanical Engineering, A J Institute of Engineering & Technology, Mangalore, India

ABSTRACT

This study employed a two-stage stir-casting technique to fabricate experimental alloys and composites using A356 + 1 wt.% Mg as the base alloy and trace copper/zinc as alloying elements and reinforcements. Peak aging conditions were applied through a solutionizing process at 520 °C and subsequent aging at 100 °C and 200 °C. A wear test was conducted using a pin-on-disk tribometer under dry sliding conditions to measure wear and frictional force. The ANSYS software simulated the wear, demonstrating a close approximation to the experimental values. The study emphasized the influence of material hardness and coefficient of friction on the wear coefficient accuracy. A higher hardness yielded closer simulated experimental values, whereas lower friction coefficients enhanced convergence. The increased contact pressure and frictional stress were accompanied by higher applied loads. The study suggests future exploration of thermal changes in frictional contact regions and incorporation of surface irregularities in realistic simulations, requiring advanced computing tools.

ARTICLE HISTORY
Received 15 February 2024
Revised 10 April 2024
Accepted 12 April 2024

KEYWORDS
Aluminum metal matrix composite; aging; ANSYS; wear; coefficient of friction

REVIEWING EDITOR
Ian Phillip Jones, University of Birmingham, United Kingdom of Great Britain and Northern Ireland

SUBJECTS
Materials Science; Metals & Alloys; Materials Processing

Introduction

The interactions between moving surfaces are at the heart of many natural phenomena. This can be observed in both natural and non-natural creations. Interest in these two physical phenomena, that is, friction and wear, arose in ancient times and reclaimed more attention in the renaissance and industrial revolution. Owing to the use of power in industrial development, the importance of wear and friction in the contact region has emerged as an important domain for research fronts (Davis, 2001; Rajesh et al., 2020; Reddy et al., 2020). All interconnected moving objects are associated with friction or wear, linking to a large amount of energy loss and failure of the parts before their life. Therefore, it is crucial to minimize friction and wear in parts that are currently used in various applications ranging from artificial organs and implants to satellites and aerospace areas for the long life of the parts. Wear can be minimized with the alteration in surface properties of the solid by surface finishing or by other 'surface engineering' processes (Alidokht et al., 2013). Wear can also be reduced by using lubricants in the case of frictional and adhesive domains (Bermúdez et al., 2001). The contact of structural elements is quite common in technology. Numerous mechanical apparatus and mechanisms are constructed using parts of a component in contact with one another (Peyre et al., 2003). A contact region was created between the tool and workpiece to remove the material during the machining process. The use of different reinforcements in a matrix can significantly improve the properties of the matrix. In the case of aluminum matrix composites (AMCs), the addition of different reinforcements can enhance the load-bearing capacity of the matrix, leading to

CONTACT Gowrishankar M C gowri.shankarmc@manipal.edu Department of Mechanical and Industrial Engineering, Manipal Institute of Technology, Manipal Academy of Higher Education, Manipal 576104, India.

improved wear resistance. This is due to the ability of the reinforcement to support the load, reducing wear rates at lower loads. However, at higher loads, the reinforcement loses its capacity to support the load, and similar wear rates are observed for unreinforced and reinforced composites (Brhane & Mekonone, 2023; Sannino & Rack, 1995).

Numerous theoretical and experimental investigations have delved into contact, friction, and wear phenomena. However, the intricate nature of tribological processes poses challenges in problem-solving. Owing to advances in numerical analysis, friction and wear modeling can be performed in computer simulations with the help of laboratory tests. Using computer simulation approaches, the physical and mechanical processes of real objects can be formed with a particularly good degree of precision. However, there is a need for efficient and reliable computational procedures for contact problems, owing to the complex nature of friction and wear. However, the accuracy of the numerical analysis can be improved. Nevertheless, new models of friction and wear should be included in the numerical calculations. New models of wear can help in better understanding and control of wear in materials. The significance of wear loss necessitates considerable effort in developing wear theories and predictive models. Meng and Ludema observed 182 equations for various types of wear (Meng & Ludema, 1995). Among them are empirical relationships, contact mechanics-based approaches, such as Archard's model, and equations based on material failure mechanisms, all of which have recently gained popularity (Singh & Vanalkar, 2012). Empirical equations are not considered in this review because they only apply to a narrow range of parameters. To date, no unified fundamental theory of wear has been established, and as a result, no single wear model is applicable in all cases. Al alloys play a significant role in the automotive and aerospace industries owing to their properties such as good tribological properties (Prasad et al., 1998; Torabian et al., 1994; Vencl et al., 2008), good recycling possibilities and high corrosion resistance (Zafar & Saeed Toor, 2022) and good thermal conductivity (Linn et al., 2023). To meet the automotive industry's demand for lightweight structures, energy efficiency, and emission reduction, it is essential to investigate advanced manufacturing techniques for A356 aluminum alloys (Bai et al., 1992; Li et al., 2021; Nithesh et al., 2023; Shabestari & Moemeni, 2004).

Põdra and Andersson (1999) described an approach for simulating wear using the commercial finite element (FE) software ANSYS. They utilized the linear wear law and Euler integration scheme as part of their modelling and simulation processes. The Lim and Ashby wear maps were utilized for both experimental and numerical studies in order to determine the wear process in an unlubricated steel contact involving a spherical pin-on-disk. The study showed that, for a given geometry and loading conditions, the wear coefficient and sliding distance change equivalency may be used to interpret the wear simulation results from finite element analysis (FEA). Benabdallah and Olender (2006) investigated wear phenomena by employing FEA with ANSYS 6.1 software to model the wear equation governing the geometry and wear profile of a polyoxymethylene (POM) pin in sliding contact with a revolving steel disk. They validated the modeling process by comparing it with a theoretical solution for a simpler case, and then compared the results with experimental data obtained under various conditions, including contact pressure, sliding length, and sliding speed. The FEA model incorporated Coulomb friction and a wear algorithm based on the Holm-Archard equation but did not account for frictionally induced heating. The simulation revealed that the pin's wear profile developed an inclination owing to uneven pressure distribution at the contact zone, constrained by ideal boundary conditions that limited the pin's radial edges to vertical movement only. The modeled results were in good agreement with the experimental observations, and the wear profile stabilized after reaching a steady-state equilibrium angle of inclination. This stabilization was associated with the end of the run-in period. The simulation was also used to predict the geometrical effects of the pin's aspect ratio (AR) on wear, and it was found that beyond a critical AR of 1.9, uneven wear increased significantly.

Shi et al. (2020) studied the importance of accurately estimating tool wear morphology, which helped in investigating the impact of tool wear on cutting parameters and production costs. This work addressed the complex problem of tool wear prediction by introducing a novel method to model real chip production and wear evolution using a three-dimensional FE model. In order to improve the accuracy of simulation results concerning wear rate, the study took into account factors including temperature distribution, stress, and worn tools. To validate the accuracy of the proposed model, they conducted cutting experiments involving turning AISI1045 using uncoated carbide tools. A comparison between the experimental and simulation results revealed good agreement, demonstrating the capability of the proposed model to predict the tool wear. Subsequently, the validated FE

model was employed to investigate the effect of worn tools on cutting performance, including the actual cutting rake, stress distribution, cutting force, and temperature.

In a study by Vijay et al. (2021), the wear characteristics of an yttrium-stabilized zirconia coating on an Al6061 aluminum alloy were examined using FEA. Aluminum alloy 6061 was chosen as the substrate material because of its favorable strength-to-weight ratio, making it suitable for thermal barrier coating (TBC) applications. The analysis employed friction and wear coefficients obtained from a continuous sliding motion between the yttrium-stabilized zirconia layer and an aluminum oxide disk. ANSYS software and the Archard wear model were used for the numerical analysis, enabling the assessment of key tribological properties, such as contact pressure, frictional tension, and wear thickness. In our previous work, the presence of Mg, Cu, and Zn to A356 as alloying elements improved the material's hardness and wear resistance significantly in both the as-cast and age-hardened states. According to the study's findings, the A356 alloy's overall wear resistance was improved along with its coefficient of friction when small amounts of copper and zinc were added as alloying agents in addition to the precipitation hardening procedure. Peak aging at 100 °C and 1 wt.% Cu as alloying element to A356 alloy resulted in maximum wear resistance property (Kashimat et al., 2023). Various reinforcement additions to the matrix A356 led to improvements in its wear properties, making it more suitable for industrial applications. The presence of low-melting copper-coated zinc particles and Cu as reinforcements in the A356 composites facilitated age hardening under both as-cast and age-hardening treatments. 0.5 wt.% copper-reinforced composite aged at 100 °C, exhibited increase in hardness and displayed substantial enhancement in wear resistance as compared as cast A356 alloy (Nithesh et al., 2023).

The primary objective of this study is to conduct a wear simulation of a pin-on-disk model configuration. To achieve this, FEA techniques were employed to simulate the frictional interaction between the pin and the disk. This simulation aims to provide valuable insights into the wear and tear processes that occur in this specific configuration. To validate the accuracy and reliability of the FEA results, we compared them with experimental data obtained through physical testing. This comparative analysis allowed for the assessment of the congruence between computational predictions and real-world observations, providing a robust basis for evaluating the performance of the FEA model. Furthermore, an integral part of this study involved evaluating various tribological characteristics, including the frictional stress and contact pressure exerted on the pin material during the simulation. These parameters play a critical role in understanding the wear behavior and performance of the pin-on-disk configuration.

Methodology

In this study, a two-stage stir-casting technique was employed to fabricate experimental alloys and composites using the A356 + 1 wt.% Mg as the base alloy/matrix and trace amounts of copper and zinc as alloying elements/reinforcement materials. The detailed explanation of preparation of alloy and composites were already explained in our previously published literature (Kashimat et al., 2023; Nithesh et al., 2023). Table 1 shows the fabricated alloys and composites with the respective compositions used to conduct the wear tests. To maintain Zn as a separate identity in the composite specimens, Zn particles were coated with 10–12 μm copper using an electrolytic coating technique.

The fabricated alloys and composites were subjected to peak-aging conditions in a series of steps. Initially, they were subjected to solutionizing at 520 °C for 2 h and then rapidly quenched in water at 60 °C. Subsequently, aging was performed at two different temperatures, 100 °C and 200 °C, for various time intervals to determine the peak-aged hardness values. Hardness test were carried at room temperature as per ASTM E384 standard using a Matzusawa micro Vickers hardness tester, with a load of 200 gmf and a dwell time of 15 s. The average of five concurrent hardness numbers was obtained from the indentations to represent the variability in the hardness measurements (Kashimat et al., 2023; Nithesh et al., 2023).

Wear tests were conducted under as-cast and heat-treated conditions following ASTM G99-04 standards utilizing pin-on-disk wear testing equipment under dry sliding conditions. Prior to the wear tests, cylindrical pins made of the alloy and composites of different diameters were prepared through a wire-EDM promfcess and used as test specimens. During the experiment, the applied load ranged from to 20–60 N while maintaining a constant sliding speed of 1 m/s

Table 1. Fabricated alloys and composites.

Material	Compositions
A	A356 + 1 wt.% Mg
A1 alloy	A + 0.5 wt.% Zn + 0.5 wt.% Cu
A2 alloy	A + 1wt.% Cu_p
C1 composite	A + 0.5 wt.% Cu coated Zn_p+0.5 wt.% Cu_p
C2 composite	A + 1 wt.% Cu

and a sliding distance of 3000 m. For the pin specimen, flat-type shapes made from the A356 alloy and composites with a height of 30 mm were used in the study, each having a diameter of 8 mm. The equipment simultaneously recorded the wear (μm) and frictional force, with measurements taken at a track radius of 60 mm (Kashimat et al., 2023; Nithesh et al., 2023; Yu et al., 1997). Figure 1 shows the pin-on-disk tribometer used in the current study.

To validate the experimental results, ANSYS software was employed to simulate and assess the wear. ANSYS is a software application that works using the FE method to simulate engineering problems. Creating or importing the geometry, setting up the FEM Model, and specifying the element kinds, material characteristics, and problem interactions are the most important initial tasks in any FEM software. In the solving steps, the software generates the solutions by taking the conditions fed in the preprocessing stage and solving them using the solver applications, and computes the output for the unknown variables such as total deformation, stress–strain induced, frictional behavior, pressure distribution, wear rate, and contact pressure. The post-processing stage involves visualizing the results obtained from simulations. This includes generating graphs and plots to visually represent the solutions obtained during the simulation process. The simulation was performed in the transient structural analysis module of ANSYS Workbench 19.2.

Steps followed in FEM simulation of this project are as follows:

3D Model of pin-on-disk tribometer

The geometric model of the pin and disk can be created using modeling software, or it can be created in the designer module of the commercially available FEA software. If geometry is created using commercially available modeling software, then the geometry must be imported with compatible file types to the FEA software and then proceed with the work. In this study, the designer module of ANSYS workbench was used to create the geometry of the pin and disk with their respective dimensions.

Figure 2(a) shows the experimental set up close view of pin and disk arrangement. Where as In the ANSYS Design Modeler, a 3D model of the pin and disk was created, as shown in Figure 2(b). Owing to the simplicity of the pin and disk geometry, ANSYS Design Modeler was chosen for model creation. The pin and disk's specified dimensions were met by configuring the unit system in the Designer Modeler to millimeters (mm). The disk, precisely modeled with a diameter of 100 mm and thickness of 7 mm, is depicted in the resulting 3D models below:

ANSYS engineering data was used to establish the materials for this project. Specifically, the disk was composed of hardened EN32 steel. For the A356 alloy utilized in this module, the engineering data included an elastic modulus of 72.4 GPa and Poisson's ratio of 0.33, which was consistent across all specimens involved in the experiment. The densities of the specimens are listed in Table 2.

Following the creation of these materials, it was essential to assign the respective material properties to the pin and disk components. Additionally, to properly configure the model for the simulation, it was necessary to specify the behavior of the pin as flexible and designate the disk as rigid.

Define contact region

Defining the contact between the pin and disk is a pivotal aspect of this project. In ANSYS, connection features offer support for creating various connections,

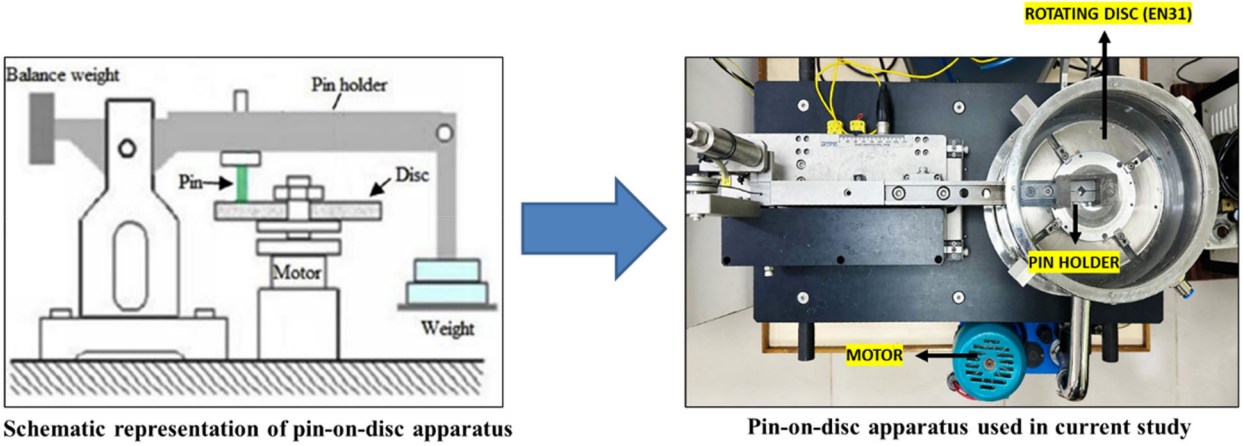

Figure 1. Pin-on-disk tribometer.

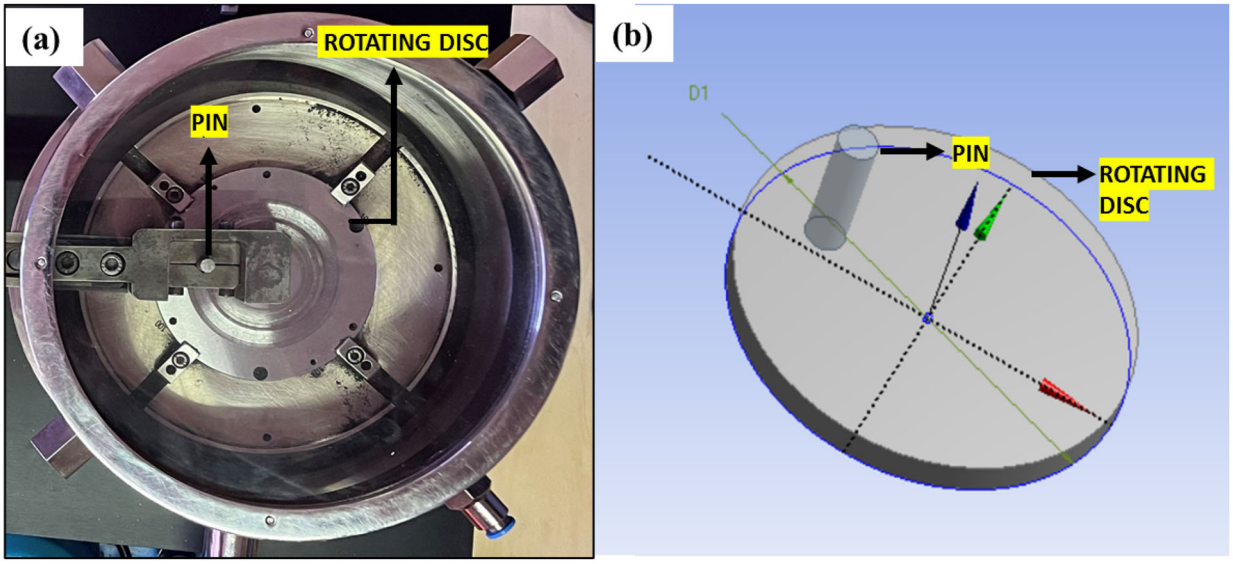

Figure 2. (a) Experimental setup of pin and disk; (b) 3D model of the pin and disk.

Table 2. Density values of specimens.

Specimen	Density (g/cc)
A	2.6509
A1	2.6972
A2	2.7004
C1	2.6857
C2	2.6898

including joints, contacts, springs, beam connections, and welds. These connections can be established either manually or automatically within the software depending on the assembly and requirements. ANSYS also provides the option to manually override these connections, if necessary. The contact regions manifest as subordinate objects under the connection group object, affording control over various parameters of the contact pair. To accurately simulate the interaction between the pin and disk, it is essential to select the type of frictional contact.

The initial step in creating contact involves selecting the bodies to define which one should be designated as the contact body and which one is the target body. In this project, with a specific focus on the pin side, the pin was chosen as the contact body, whereas the disk was designated as the target body. It is important to note that the entire body is not selected as the contact/target; rather, only the specific faces where contact interaction occurs are chosen as the contact and target surfaces. It is crucial to emphasize that the coefficient of friction must be provided as an input during the contact creation process. The coefficient of friction value is derived from the experimental data and is updated in the coefficient of friction tab within the software. Table 3 displays the average coefficient of friction values for specimens A, A1, A2, C1, and C2 under various aging conditions. These values are essential for accurately modelling the frictional contact in the simulation.

In configuring the contact behavior, it is important to set it to 'Asymmetric' since the contact involves interaction between a flexible pin and a rigid disk. Under the advanced settings tab, the formulation method should be set to 'Augmented Lagrange's Method' to address contact problems effectively. Additionally, the detection method should be specified as 'Nodal normal to target' under the detection method option. The 'Normal stiffness factor' should be set to 0.1. The Contact Tool is a valuable resource for checking the status of a created contact. This provided initial information about the contact to proceed further. If the contact appears in gray, yellow, orange, or red, it is essential to investigate whether these colors may indicate errors that occur during the contact creation process. These color-coded indications help identify and resolve potential issues with contact.

While ANSYS may not have a built-in, direct method for simulating wear mechanisms, it offers the flexibility to integrate commands and execute them. To invoke Archard's wear for the contact definition between the pin and disk, a script can be used, typically involving the commands TB and WEAR. In this script, the wear coefficient (K) should be specified, which is typically obtained experimentally. The hardness value (H) was expressed in units of N/mm^2. The exponents 'm' and 'n' represent the exponents of pressure and velocity, respectively, and their values are usually set to 1 in this context. By

Table 3. Experimental values of wear and coefficient of friction for specimens (Kashimat et al., 2023; Nithesh et al., 2023).

		Coefficient of friction			Wear (microns)		
Specimen	Load in N	As-cast	Aged at 100 °C	Aged at 200 °C	As-cast	Aged at 100 °C	Aged at 200 °C
A	20	0.64	0.52	0.53	54	38	47
	40	0.65	0.56	0.6	83	62	74
	60	0.71	0.59	0.6	127	101	119
A1	20	0.66	0.53	0.55	50	41	46
	40	0.66	0.61	0.63	75	61	69
	60	0.7	0.57	0.62	120	102	111
A2	20	0.63	0.5	0.55	46	21	40
	40	0.62	0.59	0.62	64	41	52
	60	0.68	0.54	0.59	102	26	97
C1	20	0.42	0.32	0.36	45	32	36
	40	0.38	0.3	0.34	64	42	54
	60	0.39	0.32	0.37	86	51	65
C2	20	0.36	0.3	0.33	38	22	29
	40	0.28	0.26	0.27	58	31	49
	60	0.3	0.28	0.29	72	22	51

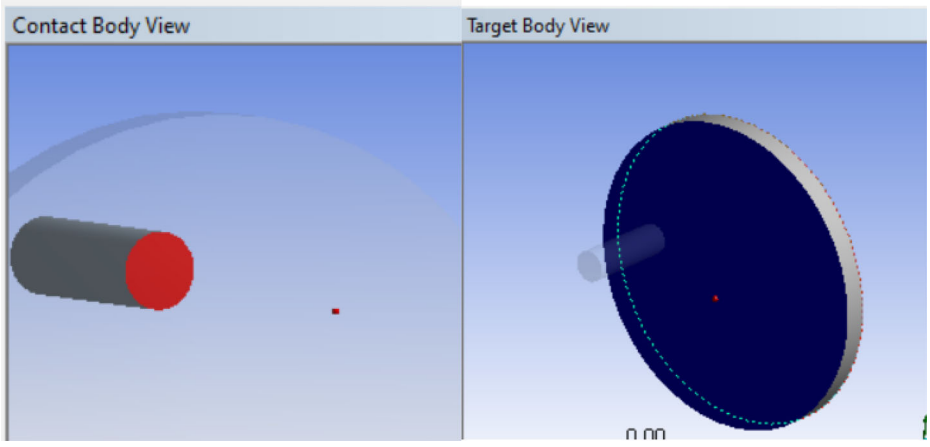

Figure 3. Contact body view and target body view.

integrating these commands and values, we can simulate wear effects in ANSYS analysis, allowing for a more comprehensive understanding of the contact behavior and wear patterns.

In the pin-on-disk test, the disk was rotated according to the specified test conditions. To simulate disk rotation, it was necessary to create a joint that provided the rotational capability. The joint creation process was typically performed under the 'Connection' tab. A Revolute joint with a connection type of 'Body-Ground' was created, allowing rotation specifically about the *z*-axis while constraining other degrees of freedom. This setup accurately modeled the rotational behavior of the disk in the pin-on-disk test. Figure 3 shows a view of the contact body and target body.

Meshing of the 3D model

Meshing was the most prominent factor for obtaining the most approximate value in the solution in the FEA. The model was optimized by altering the nodes and elements using different methods, such as edge sizing, body sizing, and face meshing. The number of nodes and elements were finalized while considering the solution time.

Mesh generation involves creating a polygonal or polyhedral mesh to approximate a given geometric domain. In this study, tetrahedra, pyramids, prisms, and hexahedra were utilized to construct three-dimensional meshes for FEA. While the finite volume approach permits the use of any polyhedral shape, finite difference methods typically necessitate piece-wise-organized arrays of hexahedra, commonly referred to as multiblock structured meshes. In essence, a mesh is a discretization of a domain that exists in one, two, or three dimensions. Structured meshes are characterized by regular connectivity, expressed as a two- or three-dimensional array, limiting the element options to quadrilaterals in 2D and hexahedra in 3D. In the present study, the meshing method employed was multizone meshing, and mesh sizing was performed using face sizing. The multizone mesh approach automatically separated

the geometry into free (unstructured) and mapped (structured) zones. Where possible, it automatically generated a pure hexahedral mesh and filled more complex sections with an unstructured mesh. To effectively control the mesh size for specific faces or groups of faces, face sizing was applied to these areas. Under the default meshing settings, the physics preference was set to nonlinear mechanical, and the element size was set to 3 mm. The same conditions were applied to mesh all specimens in the A, A1, A2, C1, and C2 configurations. Figure 4 shows the meshed model of the specimen.

Applied load and boundary condition

Boundary conditions play a crucial role in FEA, as they define the constraints and interactions that the analyzed system undergoes. These boundary conditions are necessary to achieve a realistic simulation and to obtain a unique solution. They serve several important purposes, including

a. Constraining motion: Boundary conditions are used to restrict the degrees of freedom of the model, which helps simulate real-world constraints on the system.
b. Simplifying the model: This model can be simplified by specifying how certain parts of the system interact with each other or with external forces.
c. Realistic load conditions: Boundary conditions are essential for applying realistic load conditions to the model, ensuring that the analysis accurately represents the physical behaviour of the system.

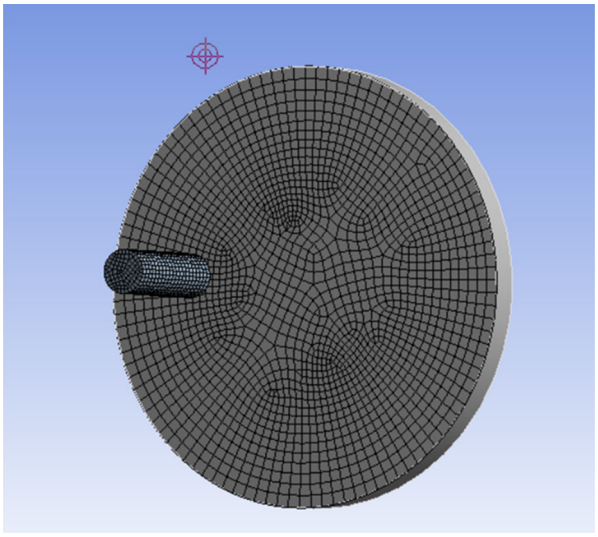

Figure 4. Meshed model.

In this particular study, the boundary condition was applied to the pin by providing it with a cylinder support, where the axial direction was set to free, as shown in Figure 5. This boundary condition ensures that the pin behaves as expected in the simulation considering its real-world constraints and interactions. Force was applied to the pin according to the experimental conditions. Force was applied in the *z*-direction. The rotation of the disk was imparted under the joint load condition. Specifically, a revolute joint created under the connection load is assigned a joint load of type specified as the rotational velocity. The rotational velocity was set at 200 rpm, which was equivalent to approximately 20.944 rad per s. This load condition ensured that the disk rotated at the desired speed during the simulation. The analysis was executed for 1 s, with an initial time step of 0.01 s. This choice of analysis time and time step was made while considering the constraints posed by the available computational resources. Smaller time increments required more processing resources, therefore a compromise between accuracy and computational efficiency was necessary. In this study, when a time of 5 s was considered, the time required to complete the run was somewhere between 30 to 40 min. When 15 s was considered, the run time was between 50 min to 1 h. However, these times considered did not affect the results i.e. a very small difference in the results is observed (order of 0.01) when compared with the results obtained for 1 s. Because of this reason, 1 s was considered and carried throughout.

Post-processing

This stage of the FEA solution involves obtaining results either graphically or through plots using the available result plot trackers within the application. The analysis focused on post processing aspects, including the following parameters: contact pressure (MPa), frictional stress, contact status, volume loss, and sliding distance. The simulation was repeated for all specimens under all load conditions using the solution object provided within the module.

Results and discussion

Figure 6 shows a bar graph of the considered hardness values. The experimental results as shown in Table 3, revealed that the wear rate of both the as-cast and heat-treated alloys and composites increased with the applied load, consistent with Archard's wear law. In both the as-cast and heat-

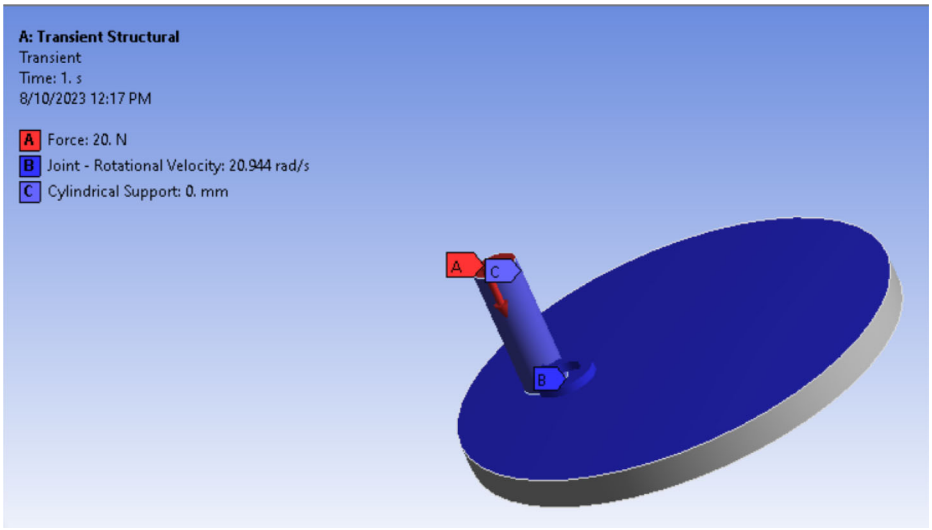

Figure 5. Fully constrained pin-on-disk configuration.

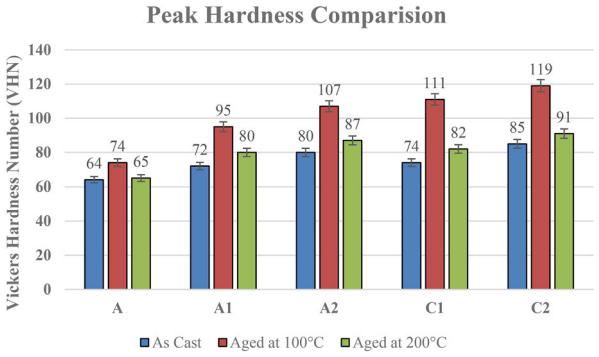

Figure 6. Hardness values of the specimens.

treated conditions, the wear rate displayed a gradual initial increase at loads up to 20 N, indicating mild wear. However, the wear rate experienced a significant increase when the applied load exceeded 40 N. At an applied load of 60 N, severe wear was observed, marked by the transfer of material from the pin to the rotating steel disk. Severe wear entails substantial metal transfer from the pin to the counter face during sliding, resulting in a higher mass loss and wear rate (Gowri Shankar, 2017; Shettar et al., 2021; Shetty et al., 2023; Uthayakumar et al., 2013). Conversely, under mild wear conditions, the pin undergoes oxidation, generating less friction, and consequently leading to a lower wear rate. The higher hardness values of the C1 and C2 composites indicate their superior resistance to plastic deformation and material removal during sliding contact, leading to reduced wear (Mazahery & Shabani, 2013; Umanath et al., 2011). Enhanced wear resistance was achieved by increasing the hardness of the A356 alloy through heat treatment and the addition of reinforcing particles (Kashimat et al., 2023; Nithesh et al., 2023).

The wear resistance of the C2 composite was higher than that of the C1 composite under high load conditions because of the presence of copper reinforcements and the associated hardness improvement, which prevented delamination and material loss. The inclusion of 1 wt.% Cu reinforcement in the matrix enhanced effective contact between surface asperities and the opposing surface, resulting in reduced wear in the C2 composite. However, under similar load and sliding distance conditions, samples peak-aged at 100 °C exhibited significantly lower wear rates than both as-cast samples and samples peak-aged at 200 °C. This difference in the wear rates can be attributed to the kinetics of the aging process.

From the simulated results of Specimen A under loading conditions of 20, 40, and 60 N, it is evident that the contact between the pin and disk involves continuous sliding throughout the simulation. Additionally, it is noteworthy that the areas of the pin experience frictional stress, which is primarily attributed to the high contact pressure in those regions. As expected, a higher contact pressure corresponded to higher frictional stress. Volume loss due to wear was also observed in the simulation, primarily to assess the wear coefficient (Kashimat et al., 2023). It's important to note that the wear coefficient can be calculated by dividing the wear rate by the applied load. In other words, the coefficient of wear can be determined by dividing the volume loss by the product of the sliding distance and the applied load. This calculation provided valuable insights into the wear characteristics of the specimens. The experimental and simulated values are listed in Table 4.

Table 4. Experimental and simulated values for the specimens.

		Wear coefficient x 10^{-5} mm^3/Nm (Exp)			Wear coefficient x 10^{-5} mm^3/Nm (Simulated)			Absolute % Error		
Specimen	Load (N)	As-cast	Aged at 100 °C	Aged at 200 °C	As-cast	Aged at 100 °C	Aged at 200 °C	As-cast	Aged at 100 °C	Aged at 200 °C
A	20	3	2.25	2.62	4.1	2.6	3.53	26.82	15.41	25.77
	40	4.49	3.37	3.93	6.1	3.98	5.29	26.39	15.32	25.7
	60	6.74	5.12	6.12	9.22	6.06	8.24	26.73	15.51	25.72
A1	20	2.62	2.25	2.25	3.27	2.13	2.53	19.87	5.33	11.06
	40	4.12	3.18	3.56	5.15	3.01	4	20	5.34	11
	60	6.37	5.49	5.99	7.97	5.2	6.65	20.07	5.28	9.92
A2	20	2.25	1.12	2.25	2.6	0.97	2.39	13.46	13.39	5.85
	40	3.37	2.25	2.81	3.9	1.95	2.99	13.58	13.33	6.02
	60	5.49	1.37	5.12	6.36	1.18	5.46	13.67	13.86	6.22
C1	20	2.62	1.87	2.25	3.19	1.51	2.47	17.86	19.25	8.9
	40	3.56	2.25	2.81	4.33	1.82	3.08	17.78	19.11	8.76
	60	4.62	2.75	3.5	5.62	2.23	3.84	17.79	18.9	8.85
C2	20	1.87	1.12	1.5	2.04	0.87	1.52	8.33	22.32	1.34
	40	3.18	1.12	2.62	3.47	0.87	2.67	8.35	22.32	1.87
	60	3.87	1.12	2.62	4.22	0.87	2.67	8.29	22.32	1.87

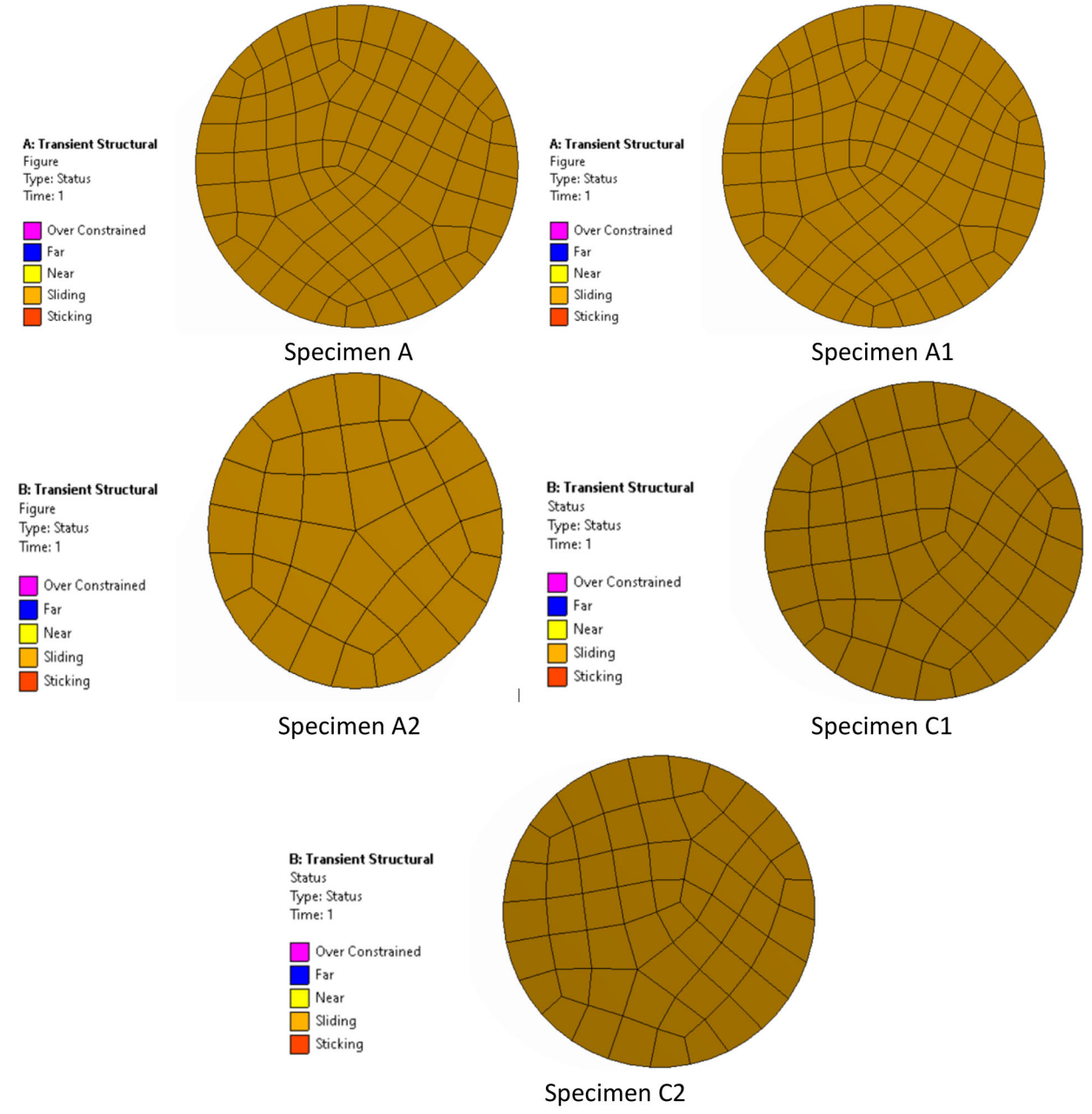

Figure 7. Contact status of the specimen.

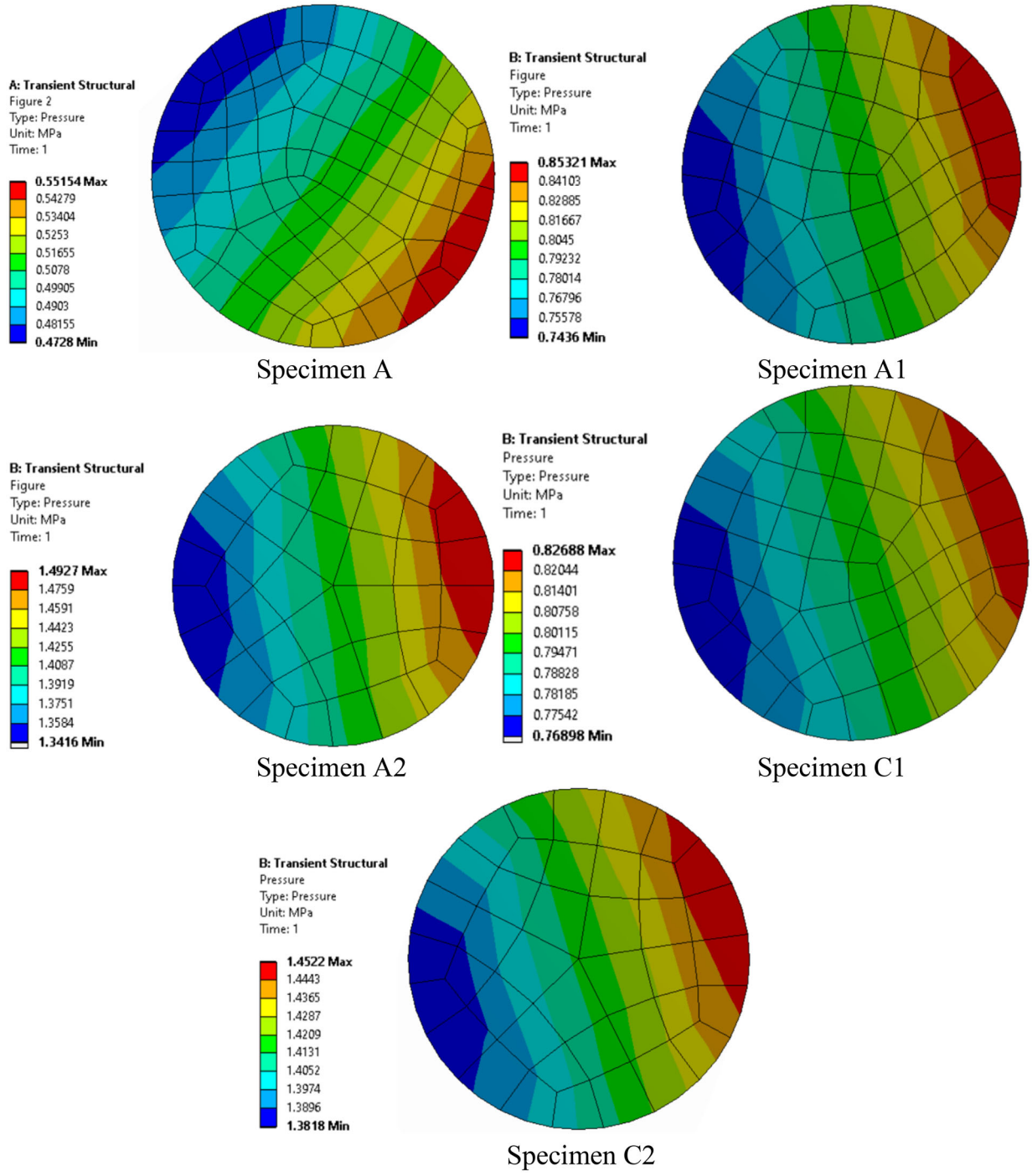

Figure 8. Contact pressure for the specimens under the load condition 40 N, as cast condition.

The observations indicate an average percentage error of approximately 34% between the values obtained from the experiment and those obtained through simulation. Specimen A, both in its as-cast and aged conditions at 200 °C, exhibited a higher percentage difference in values than Specimen A aged at 100 °C. This suggests that the simulation results were less accurate or less aligned with the experimental results for Specimen A under the former conditions. Factors contributing to this difference may include material properties, boundary conditions, and other aspects of the simulation setup that require further investigation and refinement.

A comparison between the simulated and experimental values revealed varying levels of alignment for different specimens and conditions. Specimen A1, aged at 100 °C, showed a close match with only a 6% error in the simulated values. However, when the specimen was aged at 200 °C, the error increased by approximately 18%. In the case of Specimen A2,

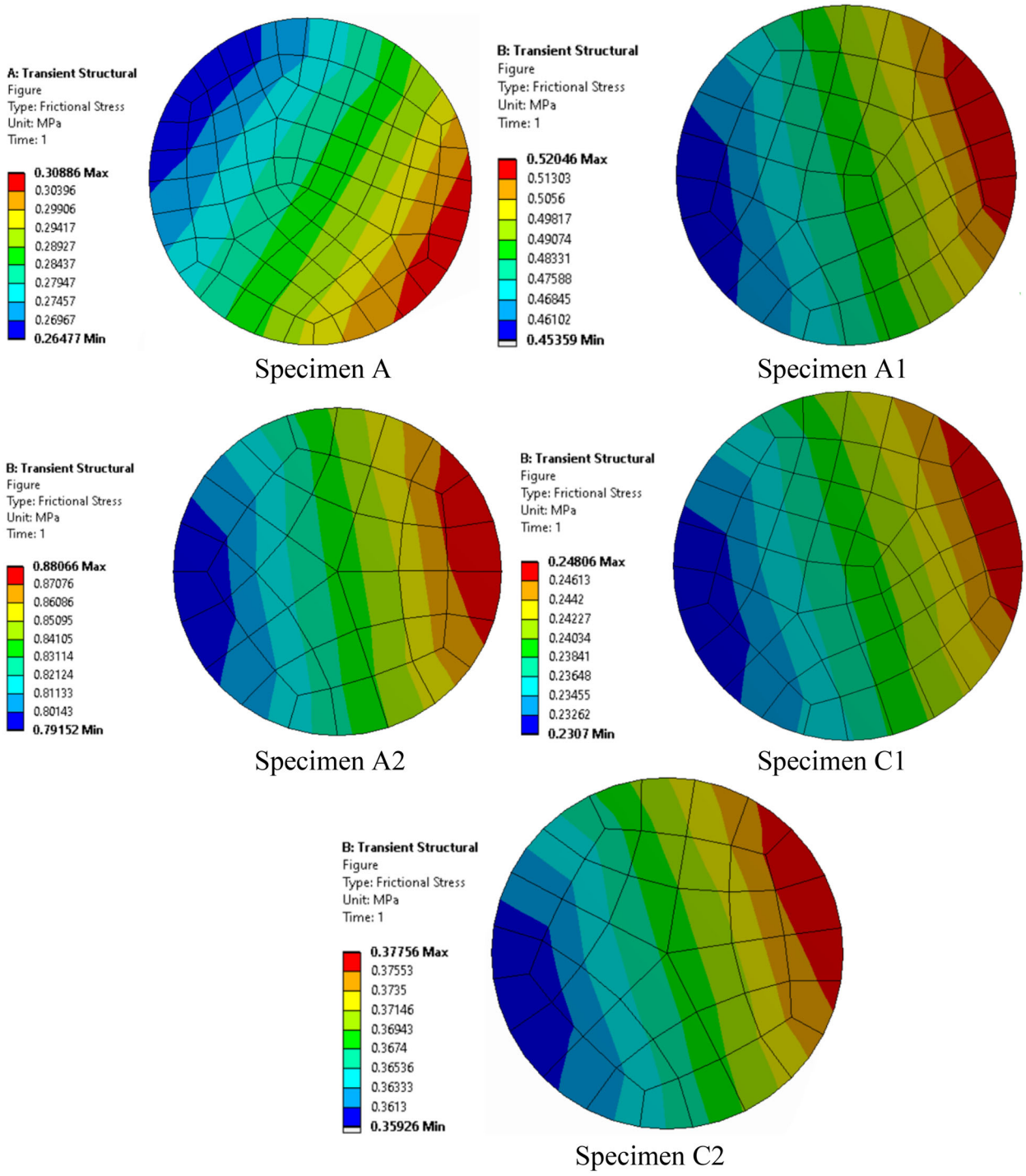

Figure 9. Frictional stress for the specimens under the load condition 40 N, as cast condition.

both the as-cast and aged conditions (100 °C and 200 °C) exhibited discrepancies, with errors ranging from 12% to 19% compared to the experimental results.

With an error rate of 23%, the simulated values for Specimen C1 showed a significant disparity in the as-cast state. But the inaccuracy dropped to 19% when the material was aged at 100 °C. The simulation's better performance for Specimen C1 aged at 200 °C is especially impressive, since the error dropped dramatically to just 8.75%. In contrast, Specimen C2 demonstrated a closer alignment between the simulation and experimentation across all conditions, including as-cast, aged at 100 °C, and aged at 200 °C, as well as load variations of 20, 40, and 60 N. In these cases, the percentage error in the simulated values was considerably lower, indicating a more accurate representation of the experimental data.

Upon analyzing the simulation results for specimens A, A1, A2, C1, and C2 under various conditions (as-cast, aged at 100 °C, and aged at 200 °C), Specimen A had notably lower hardness values than the other specimens. In addition, it exhibited a considerably higher coefficient of friction. This distinctive combination of low hardness and high friction coefficients may have contributed to the larger percentage of errors observed in the simulated values. It is worth noting that such high friction coefficients introduced as input parameters in simulation software can lead to numerical challenges. The differences between the experimental and simulated values tended to be smaller for the specimens with higher hardness values. Notably, in this study, the specimens aged at 100 °C displayed greater hardness than the as-cast and specimens aged at 200 °C (Kashimat et al., 2023; Nithesh et al., 2023). Consequently, these specimens exhibit less disparity between the simulated and experimental values. Specimens C1 and C2, characterized by lower coefficients of friction, displayed simulated values that closely approximated the experimental results. The FEA software achieved a high degree of accuracy in these cases with minimal differences between the simulated and experimental values. Figure 7 shows the contact status of the specimens obtained from the software. Figure 8 shows the contact pressure for the as-cast specimens under a load of 40 N. Figure 9 depicts the frictional stress for the as-cat specimens under a load of 40 N. In this study, the sliding contact status was noted for each specimen. Figure 8 shows that the contact pressure is slightly greater at the edges than overall. The remaining portion exhibited a slightly smooth distribution of the contact pressure. This suggests that the edges may have been the source of wear initiation. This location was also determined to have the largest frictional stress owing to the higher contact pressure, as shown in Figure 9. It is also worth noting that there is a direct correlation between the applied load and contact pressure; that is, as the applied force rises, so does the contact pressure, which raises the frictional stress. In every specimen, under every choice of experimental settings, this pattern was noted.

Conclusions

In this work, a pin-on-disk configuration 3D model was created, and a simulation was carried out successfully. This project focused on pins. Because the study was on pin material, the disk was made rigid and its deformation and changes were not concentrated. The assumption of a rigid disk provides a more convincing result than other methods.

Modeling the configuration and implementing friction-based contact models is simplified within ANSYS. The software was utilized to simulate the coefficient of wear value, which was subsequently compared with experimental data. The findings revealed a close alignment between the simulated and experimental values, demonstrating the effectiveness of the simulation approach.

This study emphasized both the coefficient of friction and the material hardness. It was observed that as the material hardness increased, the simulated wear coefficient closely matched the experimental results. Likewise, lower coefficients of friction led to greater convergence between the simulated and experimental values. Additionally, minimal pin deformation was observed during the experiments.

This study also highlighted the coefficient of friction and hardness of the material. When the hardness of the material was high, the simulated value of the wear coefficient was close to the experimental value. Similarly, when the coefficient of friction was low, the values are converging with the experimental values. The deformation of the pin was very small.

It is also observed that the higher contact pressure is observed at the contacts when the higher loads are applied. This, in turn, increased the frictional stress at the contact region. These results open the way for future studies on thermal changes associated with frictional contact regions. In the future, it will be necessary to incorporate the surface irregularities of the model in software applications and carry out simulations, which will be a realistic approach that also requires highly computing and technologically advanced software.

Author contribution

Nithesh K: experiment work; Gowrishankar M C: designing the methodology, drafting of paper; Sathyashanakara Sharma: interpretation and analysis; Ananda Hegde: revising the manuscript; Shamanth Bhat M: methodology; Rajesh Nayak: editing the manuscript; Srinivas D: eeview of manuscript.

Disclosure statement

No potential conflict of interest was reported by the author(s).

About the authors

Dr Nithesh K is working as Assistant Professor in the Department of Mechanical Engineering, A J Institute of Engineering & Technology, Mangalore, He holds Ph.D in mechanical engineering. He has published 6 papers in journals and conferences. His area of interest includes heat treatment of metals.

Dr. Gowri Shankar, holds a Ph.D. from the Manipal Institute of Technology, and currently is a Professor at the Department of Mechanical and Industrial Engineering of the same institute. His main areas of research include Machining of Materials; Heat Treatment of Ferrous and Non-Ferrous Materials.

Dr. Sathyashankara Sharma is working as Senior Professor and Head in the Department of Mechanical & Industrial Engineering, MIT, MAHE, Manipal. He holds B.E. (Mechanical), M.Tech. (Materials Engineering) and Ph.D. (Materials Engineering) degrees. He has more than 35 years of teaching experience. His area of interest includes materials engineering, heat treatment of metals and composites and deformation behavior of metals and composites. He has published more than 150 papers in journals and conferences.

Dr. Ananda Hegde is working as Associate Professor in the Department of Mechanical & Industrial Engineering, MIT, MAHE, Manipal. He holds Ph.D in mechanical engineering. He has more than 10 years of teaching experience. His area of interest includes materials engineering, heat treatment of metals. He has published more than 30 papers in journals and conferences.

Shamath Bhat, holds B.Tech in Mechanical Engineering and M.Tech in Manufacturing Engineering at Manipal Institute of Technology.

Dr. Rajesh Nayak, holds a Ph.D. from the Manipal Institute of Technology, and currently is an Associate Professor at the Department of Mechanical and Industrial Engineering of the same institute. His main areas of research include Machining of Materials, Cryogenic machining, Composite materials, Heat Treatment of Ferrous and Non-Ferrous Materials.

Srinivas D holds PhD in Mechanical Engineering. His main areas of research include Materials characterization, aluminum matrix composites.

ORCID

Gowrishankar M C http://orcid.org/0000-0001-9951-800X
Sathyashanakara Sharma http://orcid.org/0000-0001-8995-1563
Ananda Hegde http://orcid.org/0000-0002-8256-8665

Data availability statement

The data that support the findings of the study are available from corresponding author, upon reasonable request.

References

Alidokht, S. A., Abdollah-Zadeh, A., & Assadi, H. (2013). Effect of applied load on the dry sliding wear behaviour and the subsurface deformation on hybrid metal matrix composite. *Wear*, *305*(1-2), 291–298. https://doi.org/10.1016/j.wear.2012.11.043

Bai, B. N. P., Ramasesh, B. S., & Surappa, M. K. (1992). Dry sliding wear of A356-Al-SiCp composites. *Wear*, *157*(2), 295–304. https://doi.org/10.1016/0043-1648(92)90068-J

Benabdallah, H., & Olender, D. (2006). Finite element simulation of the wear of polyoxymethylene in pin-on-disc configuration. *wear*, *261*(11-12), 1213–1224. https://doi.org/10.1016/j.wear.2006.03.040

Bermúdez, M. D., Martínez-Nicolás, G., Carrión, F. J., Martínez-Mateo, I., Rodríguez, J. A., & Herrera, E. J. (2001). Dry and lubricated wear resistance of mechanically-alloyed aluminium-base sintered composites. *Wear*, *248*(1-2), 178–186. https://doi.org/10.1016/S0043-1648(00)00553-6

Brhane, A. G., & Mekonone, S. T. (2023). Numeric simulation of steel twin disc system under rolling- sliding contact. *Tribolology and Materials*, *2*(4), 181–188. https://doi.org/10.46793/tribomat.2023.019

Davis, J. R. (2001). *Surface engineering for corrosion and wear resistance*. ASM International.

Gowri Shankar, M. C. (2017). *Precipitation hardening behavior of stir cast Al6061 based hybrid* [Unpulished PhD thesis]. Manipal University, Manipal.

Kashimat, N., Sharma, S., Nayak, R., Manjunathaiah, K. B., Shettar, M., & Chennegowda, G. M. (2023). Experimental investigation of mechanical property and wear behaviour of T6 treated A356 alloy with minor addition of copper and zinc. *Journal of Composites Science*, *7*(4), 149. https://doi.org/10.3390/jcs7040149

Li, H., Jiao, L., Xu, R., Li, F., Lu, S., Qiao, Y., Li, C., & Zhang, P. (2021). Surface wear behavior and friction and wear mechanism studies of A356/3 wt.% Al_3Zr Composites. *Journal of Materials Engineering and Performance*, *30*(5), 3892–3902. https://doi.org/10.1007/s11665-021-05707-2

Linn, Z. C., Swe, W. W. M., Soe, A. K., & Latt, A. K. (2023). Experimental and numerical analysis on the thermal performance of the aluminium absorber. *Tribology and Materials*, *2*(4), 162–171. https://doi.org/10.46793/tribomat.2023.020

Mazahery, A., & Shabani, M. O. (2013). Microstructural and abrasive wear properties of SiC reinforced aluminum-based composite produced by compocasting. *Transactions of Nonferrous Metals Society of China*, *23*(7), 1905–1914. https://doi.org/10.1016/S1003-6326(13)62676-X

Meng, H. C., & Ludema, K. C. (1995). Wear models and predictive equations: their form and content. *Wear*, *181-183*(2), 443–457. https://doi.org/10.1016/0043-1648(95)90158-2

Nithesh, K., Nayak, R., Hande, R., Sharma, S., Gowri Shankar, M. C., & Doddapaneni, S. (2023). Dual role of trace elements in magnesium dissolved age hardened A356 alloy on microstructure and peak micro hardness. *Manufacturing Review*, *10*(5), 5. https://doi.org/10.1051/mfreview/2023003

Nithesh, K., Sathyashankara, S., Rajesh, N., Gowrishankar, M. C., Karthik, B. M., & Doddapaneni, S. (2023). Wear behaviour analysis of heat treated A356 composite with

copper and copper-coated zinc as reinforcements. *Materials Research*, *26*(1), 1–12.

Peyre, P., Sollier, A., Chaieb, I., Berthe, L., Bartnicki, E., Braham, C., & Fabbro, R. (2003). FEM simulation of residual stresses induced by laser peening. *The European Physical Journal Applied Physics*, *23*(2), 83–88. https://doi.org/10.1051/epjap

Põdra, P., & Andersson, S. (1999). Simulating sliding wear with finite element method. *Tribology International*, *32*(2), 71–81. https://doi.org/10.1016/S0301-679X(99)00012-2

Prasad, B. K., Venkateswarlu, K., Modi, O. P., Jha, A. K., Das, S., Dasgupta, R., & Yegneswaran, A. H. (1998). Sliding wear behavior of some Al-Si alloys: Role of shape and size of Si particles and test conditions. *Metallurgical and Materials Transactions A*, *29*(11), 2747–2752. https://doi.org/10.1007/s11661-998-0315-7

Rajesh, A. M. , Doddamani, S., Mohamed Kaleemulla, K., & Bharath, K. N. (2020). Dry sliding wear simulation of hybrid aluminum metal matrix composites. *Advanced Composites and Hybrid Materials*, *3*(1), 120–126. https://doi.org/10.1007/s42114-020-00133-9

Reddy, P. V., Kumar, G. S., Krishnudu, D. M., & Rao, H. R. (2020). Mechanical and wear performances of aluminium-based metal matrix composites : A review. Journal of Bio- and Tribo-Corrosion, *6*(2), 1–16. https://doi.org/10.1007/s40735-020-00379-2

Sannino, A. P., & Rack, H. J. (1995). Dry sliding wear of discontinuously reinforced aluminum composites: review and discussion. *Wear*, *189*(1-2), 1–19. https://doi.org/10.1016/0043-1648(95)06657-8

Shabestari, S. G., & Moemeni, H. (2004). Effect of copper and solidification conditions on the microstructure and mechanical properties of Al-Si-Mg alloys. *Journal of Materials Processing Technology*, *153-154*(1–3), 193–198. https://doi.org/10.1016/j.jmatprotec.2004.04.302

Shettar, M., Hiremath, P., Shankar, G., Kini, A., & Sharma, S. (2021). Tribolayer behaviour and wear of aged aluminium hybrid composites. *International Journal of Automotive and Mechanical Engineering*, *18*(2), 8668–8676. https://doi.org/10.15282/ijame.18.2.2021.04.0660

Shetty, R., Hindi, J., Gurumurthy B. M., Hegde, A., Shivaprakash Y. M., Sharma, S., Amar Murthy A., & Muralishwara K. (2023). Effect of metallic reinforcement and mechanically mixed layer on the tribological characteristics of Al-Zn-Mg alloy matrix composites under T6 treatment mechanically mixed layer on the tribological characteristics of Al-Zn-Mg alloy matrix composites under T6 treatment. *Cogent Engineering*, *10*(1), 1–13. https://doi.org/10.1080/23311916.2023.2200900

Shi, Z., Li, X., Duan, N., & Yang, Q. (2020). Evalution of tool wear and cutting performance considering effects of dynamic nodes movement based on FEM simulation. *Chinese Journal of Aeronautics*, *2*(1), 1–13. https://doi.org/10.1016/j.cja.2020.08.003.

Singh, R. N., & Vanalkar, A. V. (2012). Analysis of wear phenomena in sliding contact surfaces. *International Journal of Engineering Research and Applications*, *2*(3), 2403–2409.

Torabian, H., Pathak, J. P., & Tiwari, S. N. (1994). Wear characteristics of Al-Si alloys. *Wear*, *172*(1), 49–58. https://doi.org/10.1016/0043-1648(94)90298-4

Umanath, K., Selvamani, S. T., & Palanikumar, K. (2011). Friction and wear behaviour of Al6061 alloy ($SiC + Al_2O_{3P}$) hybrid composites. *International Journal of Engineering Science and Technology*, *3*(7), 5441–5451.

Uthayakumar, M., Aravindan, S., & Rajkumar, K. (2013). Wear performance of Al – SiC – B_4C hybrid composites under dry sliding conditions. *Materials and Design*, *47*, 456–464. https://doi.org/10.1016/j.matdes.2012.11.059

Vencl, A., Bobić, I., & Mišković, Z. (2008). Effect of thixocasting and heat treatment on the tribological properties of hypoeutectic Al – Si alloy. *Wear*, *264*(7-8), 616–623. https://doi.org/10.1016/j.wear.2007.05.011

Vijay, R., Aju Kumar, V. N., Sadiq, A., & Rakesh Pillai, R. (2021). Numerical analysis of wear characteristics of zirconia coated aluminum 6061 alloy. *IOP Conference Series: Materials Science and Engineering*, *4*(1), 1–9. doi: 10.1088/1757-899X/1059/1/012020.

Yu, S. Y., Ishii, H., Tohgo, K., Cho, Y. T., & Diao, D. (1997). Temperature dependence of sliding wear behavior in SiC whisker or SiC particulate reinforced 6061 aluminium alloy composite. *Wear*, *213*(1-2), 21–28. https://doi.org/10.1016/S0043-1648(97)00207-X

Zafar, M. M., & Saeed Toor, Z. (2022). Corrosion degradation of aluminium alloys using a computational framework. *Tribology and Materials*, *1*(4), 150–156. https://doi.org/10.46793/tribomat.2022.019